Malaysian Journal of Catalysis

MJCat

Critical Review

The analysis of three types of zeolite as supports for LaNiO₃ catalyst in the dry reforming of methane reaction

Mostafa Rahmanzadeh
Chemical Engeneering Department, Sirjan University of technology, Sirjan, Iran
Corresponding author email: rahmanzadeh.m@sirjantech.ac.ir

GRAPICAL ABSTRACT

Methane dry reforming
On LaNiO₃/Zeolite

$CH_4 + CO_2 \longrightarrow CO + H_2$
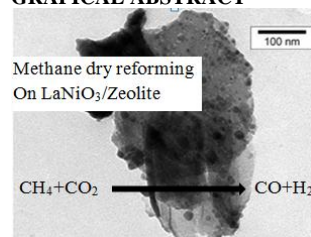
ABSTRACT

LaNiO₃/(H-MFI, H-Mor and H-MFI treated with NaOH) catalysts were prepared using the sol gel method. The XRD test shows that LaNiO₃ perovskite was formed over three supports. The TEM, SEM and EDX tests show that the Ni is dispersed very well over the supports, and the TEM test shows that the particle size of Ni is 10 nm. For all three catalysts, catalytic performance of the CO_2 reforming of methane to syngas was evaluated using a fixed-bed quartz reactor. Reactor test depicted that the LaNiO₃/(treated H-MFI) catalyst had the highest conversion of methane and CO_2. The methane conversion reaches the highest value of 13.3 wt% for Ni loading over this support.

Key words: Zeolite, dry reforming of methane, perovskite, LaNiO₃ catalysts

1.   INTRODUCTION

Among all the processes of transforming methane to syngas, the dry reforming of methane produces a lower molar ratio of H₂/CO, which suitable to be transformed to much more valuable products through various chemical processes such as Fischer Tropsch synthesis and oxo-synthesis. An alternative application of the dry reforming is the thermochemical storage and transmission of renewable energy sources. Specifically, both the solchem process and the CLEA project used the reaction of dry reforming of methane and its reverse methanation reaction by means of converting solar energy into chemical energy, which is easier to store and carry. Besides, this reaction consumes CO_2, a greenhouse gas, and processing it to higher added value products [1-4].

However, the drawback of dry reforming of methane is the deactivation of catalysts caused by carbon deposition. This serious problem could be inhibited by the use of highly dispersed metal species according to the concept of ensemble size control by using a precursor such as perovskite-like oxide ABO_3 [5-8].

These solids have high thermal and hydrothermal stability as well as high mechanical strength among other properties. However, the potential application of these oxides is limited by its small surface area, which is lower than 10 m²/g [9] and the necessary high reaction temperatures to carry out the reforming due to its endothermicity [10]. LaNiO₃ catalyst has performed well in the dry reforming of methane [11-14]. The kinetic behavior of the LaNiO₃ catalyst in the dry reforming reaction of methane has been investigated by Moradi et al. [15] and Tsipouriari et al. [16]. Investigation on

the mechanism and rate equation of dry reforming of methane on LaNiO₃ catalyst showed that perovskite structure was destroyed and thus formed La_2O_3 and Ni^0 at the condition of reaction (T $\geq$ 700 °C). Then, CO_2 with La_2O_3 produce $La_2O_2CO_3$ phase which in turn reacts with the carbon that was adsorbed on Ni^0 site and produce CO. This reaction leads to the resistant of catalyst towards carbon deposition [16-17]. Performance of this catalyst can be increased by partial substitution of promoter, either La [18-21] or Ni [22-25]. When La was partially substituted with alkaline earths, it leads to the formation of La_2NiO_4 and NiO phases. The La_2NiO_4 phase plays an important role in increasing the catalyst activity.

LaNiO₃/SBA-15 has been investigated by Rivas et al. [26]. Although specific surface area was increased from 10 m²/g to 81 m²/g for this catalyst, conversion of methane did not increase significantly (conversion of methane increased from 85% to 88%) [26]. LaNiO₃/γ-Al₂O₃ has been investigated in our previous work [27]. Usage of γ-Al₂O₃ as an acid support increases the performance of LaNiO₃ catalyst in the dry reforming of methane reaction.

In this paper, usage of various types of zeolite (H-MFI and H-Mordenite) as supports for LaNiO₃ have been investigated for the realization of action acidity and specific surface area of support in the performance of catalyst. Also, for further realization of action acidity, H-MFI zeolite has been treated with a NaOH aqueous solution which leads to the production of a very acidity support for LaNiO₃ catalyst.

2.   EXPERIMENTAL

2.1   Support Preparation

H-MFI and H-Mordenite zeolites were supplied by Merck. For varying acidity support, H-MFI zeolite has been treated with NaOH aqueous solution. This zeolite was added to an aqueous solution of NaOH (0.05 Molar, 150 cm^3) at room temperature. The suspension was heated at 80 ºC for 90 minutes. After cooling to room temperature, the solid was filtered and dried at room temperature. The obtained solid was washed using deionized water and dried at 120 ºC for 24 h. Supports were calcined by increasing the temperature from ambient temperature to 500 ºC at a rate of 4 ºC/min and maintaining that temperature for 4 h. For this paper, the treatment of H-MFI with NaOH aqueous solution for 90 minutes was denoted H-MFI90.

2.2   Catalyst Preparation

The LaNiO$_3$/(H-MFI, H-Mordenite, H-MFI90) catalyst was prepared as follows. Appropriate amounts of Ni(NO$_3$)$_2$·6H$_2$O (Merck, purity 99%) and La(NO$_3$)$_2$·6H$_2$O (Merck, purity 99%) were dissolved in ethanol with constantly heating and stirring. As soon as the complete dissolution was achieved, 2.5 mL acetic acid as polydentate ligand was added to the solution. The obtained solution was maintained under reflux condition and vigorous stirring, and then MFI was added to the solution until a green gel was formed. The produced gel was dried overnight and calcined at 750 ºC (ramp 3 ºC/min) for 4 h. The obtained catalyst was crushed and used in powder form.

2.3   Support Characterization

Acidity measurements of the zeolites prepared above were performed by temperature-programmed desorption of ammonia (NH$_3$-TPD) using a conventional flow apparatus equipped with a thermal conductivity detector (TCD). A specific amount of the sample (0.1 g) was pretreated in flowing helium (He) at 550 ºC for 1 h, cooled to 150 ºC and then exposed to NH$_3$ (20 ml/min) for 30 min. The sample adsorbed by NH$_3$ was subsequently purged with He gas at the same temperature for 1 h to remove the physisorbed NH$_3$. The TPD measurement was conducted in flowing He gas (30 ml/min) from 150 ºC, at a heating rate of 10 ºC/min, to 550 ºC and maintained at this temperature for 30 min. The evolved ammonia was trapped in a dilute H$_2$SO$_4$ solution (0.005 mol /L) located at the down-stream of the flow. Its total amount was determined by back-titration of the excess sulfuric acid with a dilute NaOH solution (0.01 mol/L).

Samples were characterized by N$_2$ adsorption/desorption isotherms to obtain the textural properties of the solid at temperature of liquid nitrogen in an automated physisorption instrument (MicromeriticsTristar 3300). Prior to the analysis, the samples were outgassed in vacuum at 300 ºC overnight.

2.4   Catalyst Characterization

Transmission electron microscopy (TEM) was carried out on a Philips EM208 instrument with an acceleration voltage of 120 kV. Specimens for TEM were prepared by ultrasonically dispersing a powder sample in ethanol. X-ray diffraction studies were performed by means of X-ray diffractometer (XRD, X'pert Philips) with Cu Ka radiation (λ=1.54052 Aº). Phase identifications were accomplished by comparing the collected spectra with the spectra in the database.

Temperature-programmed reduction (TPR) of the catalysts were carried out in a stream of 5.1 vol.%H$_2$ balanced with Ar at a flow rate of 50 ml/min using a Pulse Chemisorb 2705 instrument (micromeritics). A catalyst sample (20 mg) placed in a quartz tube was previously degassed for 2 h at 120 °C under an N$_2$ stream, and then it was cooled to room temperature. After the stream was switched from N$_2$ to reducing gas, the sample was heated by increasing the temperature linearly at a rate of 5 °C/min. The water which formed during the reduction was trapped by cooling with mixture of ethylene glycol and liquid nitrogen. The hydrogen concentration in the effluent was continuously monitored by a thermal conductivity detector (TCD).

Thermogravimetric analysis (TGA) of the sample was carried out in PL-TGA (Polymer Laboratories). Samples were heated at 10 °C min^{-1} from room temperature up to 700 °C under O$_2$ atmosphere.

2.5   Activity Test

A schematic view of the experimental setup is presented in [15]. The kinetics was studied under varying conditions in a conventional flow system consisting of a flow measuring and control system, a mixing chamber, and a fixed-bed quartz reactor (inner diameter 5 mm, height 60 cm) which was placed in an electric oven. The length of the catalyst bed was chosen approximately 2 cm to avoid the gradient temperature in axial direction of the catalyst bed. The reaction was carried out under atmospheric pressure at 700 ºC to 720 ºC. The feed and product streams were analyzed with a gas chromatograph equipped with a thermal conductivity detector and two pack columns Ms and propack Q for detecting CO, CO$_2$, and CH$_4$. The mass of the catalyst was 0.05 g, diluted with 0.45 g silicon carbide (SIC, 30-60 mesh) as inert solid.

A feed mixture with a CH$_4$/CO$_2$/He molar ratio of 1:1:8 was sent through the catalysts at a total flow of 45mL/min which corresponds to a WHSV of 4320 mL/h·g. Prior to a test, the catalysts were reduced by H$_2$ (30mL/min) at a constant heating rate of 6 °C/min from room temperature to 700 °C. This temperature was maintained during 10 hrs, then the flow rate of H$_2$ was switched off and the CH$_4$/CO$_2$ mixture was added. For the stability test, the catalyst was reduced by H$_2$ at a constant heating rate from room temperature to 700 °C. This temperature was maintained for 10 hrs and then increased to 800 °C while H$_2$ passed. Finally, the H$_2$ stream was cut and the feed was added. In all experiments, catalytic performances were evaluated by CH$_4$ and CO$_2$ conversions. These conversions were calculated as follows:

$$conversion\,(CH_4)[\%] = \frac{(CH_4)_{in} - (CH_4)_{out}}{(CH_4)_{in}} \times 100 \qquad (1)$$

$$conversion\ CO_2[\%] = \frac{(CO_2)_{in} - (CO_2)_{out}}{(CO_2)_{in}} \times 100 \qquad (2)$$

$$\frac{H_2}{CO} = \frac{(H_2)_{out}}{(CO)_{out}} \qquad (3)$$

3.   RESULTS AND DISCUSSION

3.1   Characterization of Supports

The textural characteristics of the support have been evaluated from the corresponding N_2 adsorption/desorption isotherms. Table 1 summarizes the textural properties of the solids. Compared to those support materials, the specific surface area and pore volume decreased significantly for supported catalysts. The decrease in surface area can be due to the incorporation of $LaNiO_3$ into the mesopores of support materials. The decrease of pore volume was an important evidence to prove anchoring of $LaNiO_3$ inside the pores of supports.

Table 1 Specific surface areas and pore volumes of three supports

Catalyst	BET surface area (m²/g)	Total pore volume (cm³/g)	Average pore radius (Å)
H-MFI90	391	0.389	19.88
H-MFI	460	0.353	15.01
H-Mordenite	479	0.354	14.76
LaNiO₃/ H-MFI90	215	0.257	14.35
LaNiO₃/ H-MFI	240	0.234	12.03
LaNiO₃/ H-Mor	237	0.225	12.05

NH_3-TPD was performed to monitor the acid strength and the amounts of acid sites on the H-MFI90. As shown in

Fig 1, two major NH_3 desorption peaks as well as a shoulder peak can be observed at 222 ºC (weak acid sites) and 450 ºC (trong acid sites) and 685 ºC (strong acid sites) respectively. The amount of NH_3 desorption based on the area under the first peak shown in Fig. 1 is 9.39×10^{-2} cm³ (NH_3)/g-cat, for second peak is 5.21×10^{-2} cm³ (NH_3)/g-cat and for shoulder peak is 8.76×10^{-3} cm³ (NH_3)/g-cat. Thus, the total acid sites density is 0.1 cm³ (NH_3)/g-cat. The weak acid sites are related to the external surface or to some type of extraneous material or interaction of ammonia molecules with surface oxide or hydroxyl groups by non-specific hydrogen bonding. NH_3-TPD results for H-MFI and H-Mor exhibited two peaks: the first peak due to the weak acid sites and the second peak associated with the strong acid sites (temperature of peaks showed in the Table 2).
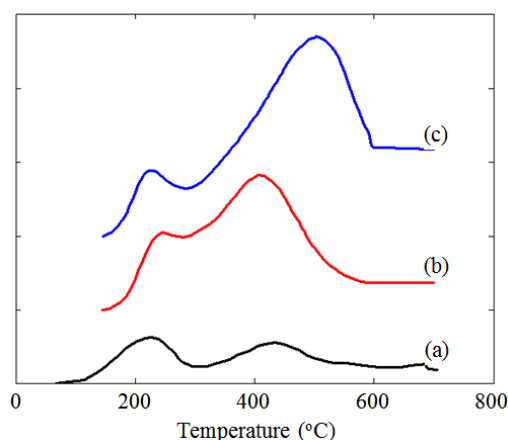
Fig. 1 NH_3-TPD response of (a) H-MFI90 (b) H-MFI and (c) H-Mo

Table 2 Summary of acid properties of H-MFI, H-M190 and H-Mor zeolites.

Solid acid catalyst	Weak acid sites Amount of NH₃ desorption (mmol) (mmol NH₃/g)	Medium acid sites Amount of NH₃ desorption (mmol) (mmol NH₃/g)	Strong acid sites Amount of NH₃ desorption (mmol NH₃/g)	Total acid sites Amount of NH₃ desorption (mmol NH₃/g)
H-MFI90	0.0014 (222 ºC)	0.0020 (450 ºC)	0.0003 (685 ºC)	0.0037
H-MFI	0.0019 (220 ºC)	-	0.0032 (425 ºC)	0.0051
H-Mordenite	0.0022 (186 ºC)	-	0.0041 (525 ºC)	0.0063

3.2   Characterization of Catalysts

The X-ray diffraction patterns of $LaNiO_3$, H-MFI, $LaNiO_3$/H-MFI, $LaNiO_3$/H-Mordenite and $LaNiO_3$/H-MFI90 are illustrated in Fig. 2. Fig. 2(a) shows XRD pattern of $LaNiO_3$ without any supports which confirms the presence of a $LaNiO_3$ perovskite-type rhombohedra structure (JCPDF 33-711).

Fig. 2(b) and Fig. 2(c) show XRD patterns of H-MFI and $LaNiO_3$/H-MFI90 respectively. With comparison among Fig. 2(a), Fig. 2(b) and Fig. 2(c), we can understand

the formation of $LaNiO_3$ over H-MFI90 support. The X-ray diffraction patterns obtained for $LaNiO_3$/H-Mordenite and $LaNiO_3$/H-MFI are presented in Fig. 2(d) and Fig. 2(e). Patterns of $LaNiO_3$ can be identified as well. As for the $LaNiO_3$/H-MFI90, its XRD curves displayed accordance with NiO. The diffraction pattern of this catalyst exhibits four broad peaks at 37.2º, 43.3º and 62.9º, corresponding to (111), (200) and (220) of NiO respectively. The XRD pattern of $LaNiO_3$/H-MFI90 presented the main diffraction peaks of H-MFI90, $LaNiO_3$ and NiO, and no other diffraction peaks appeared.

◆ NiO
● LaNiO₃
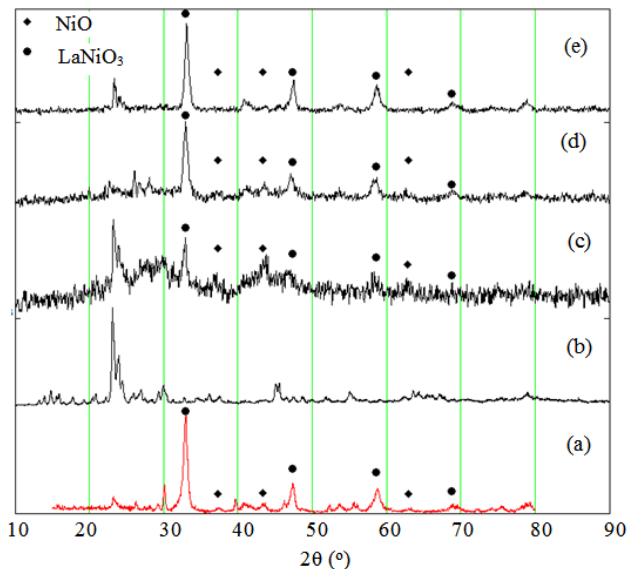
Fig. 2 X-ray diffraction (XRD) pattern of (a) LaNiO₃ calcined at 1023 K, (b) H-MFI (c) LaNiO₃/H-MFI90 at 1023 K, (d) calcined LaNiO₃/H-Mordinate and (e) calcined LaNiO₃/H-MFI
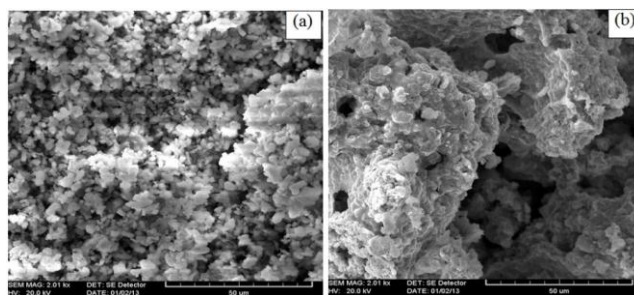
Fig. 3 SEM image of (a) H-MFI support and (b) LaNiO₃/HMFI catalyst calcined at 750 °C
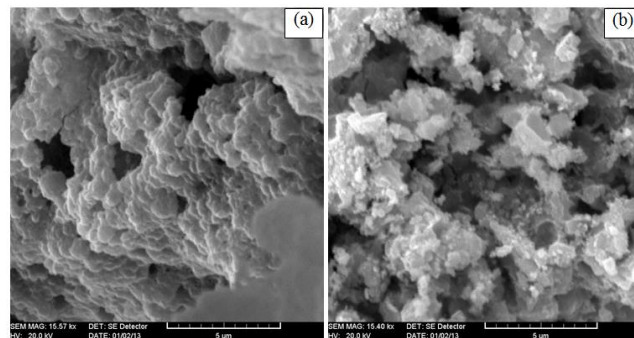
Fig. 4 SEM image of (a) LaNiO₃/H-MFI90, (b) LaNiO₃/HMordenite catalyst calcined at 750 °C.

SEM images of the H-MFI support (Fig. 3(a)) and LaNiO₃/H-MFI catalyst (Fig. 3(b)) provide clear evidence of the formation of LaNiO₃ crystalline which were well dispersed as very fine crystals on the H-MFI.

Table 3 Concentration of elements in the bulk and surface of catalysts (data for surface has been obtained from EDX analysis).

Catalyst / Element	LaNiO₃/ H-MFI		LaNiO₃/ H-Mordenite		LaNiO₃/ H-MFI90	
	Bulk	Surface	Bulk	Surface	Bulk	surface
La	4.5	17.58	4.5	17.56	4.5	19.16
Ni	4.5	20.05	4.5	20.32	4.5	21.84
Si	89.4	59.04	88	59.25	89.4	55.29
Al	1.6	2.96	3	2.59	1.6	2.8
Other elements	–	0.37	–	0.28	–	0.91

Table 4 EDX analysis of LaNiO₃/ H-MFI90 (concentration of Ni 4.5% mol) catalyst at three different points

Catalyst / Element		Mole fraction of La	Mole fraction of Si	Mole fraction of Ni
LaNiO₃ / HMFI90	Spectrum 1	14.98	60.50	22.52
	Spectrum 2	11.84	68.70	19.46
	Spectrum 3	13.02	65.31	21.67

Fig. 4(a) and (b) show SEM morphology of the LaNiO3/H-MFI90 and LaNiO3/H-Mordenite catalysts, respectively, which have been calcined at 750 ºC for 4 hrs. These catalysts exhibit a good dispersion of active site on support. It seems that impregnation of LaNiO3 on the zeolite support by ethanol solvent led to high Ni dispersion on the catalyst support surface.

Fig. 6(a) and (b) show TEM micrographs of LaNiO3/HMFI90 and LaNiO3/H-Mordenite, respectively, which have been reduced by H_2 (30 mL/min) at a constant heating rate of 6 ºC/min from room temperature to 750 ºC; and both catalysts exhibit a good dispersion active site on supports.

Fig. 7 shows TPR results for LaNiO3, H-MFI, LaNiO3/H-MFI and LaNiO3/H-Mordenite catalysts. The LaNiO3 perovskite exhibited two reduction steps: the first due to the formation of $La_2Ni_2O_5$ representing the reduction of Ni^{3+} to Ni^{2+} (390 ºC), and the second associated with reduction of Ni^{2+} to Ni^0 that remains supported on lanthanum oxide (525 ºC) [28]. Based on these results, the reduction steps are written:

$$2LaNiO_3 + H_2 \rightarrow LaNi_2O_5 + H_2O, \quad La_2Ni_2O_5 + 2H_2 \rightarrow La_2O_3 + 2Ni + 2H_2O$$
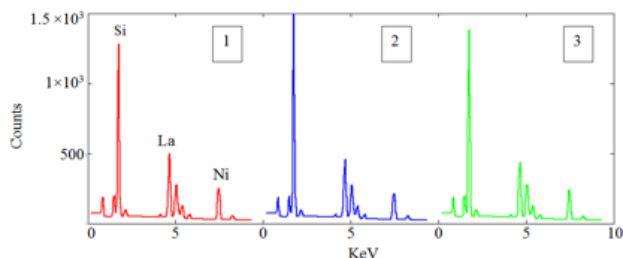
Fig. 5 Corresponding EDX spectrum for points in the table 4
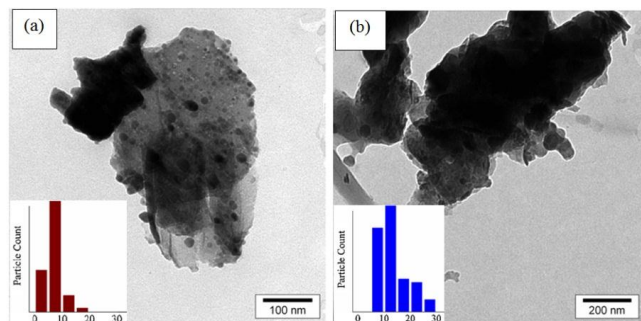
Fig. 6 TEM of LaNiO3 supported catalysts, a) the reduced LaNiO3/HMFI90, b) the reduced LaNiO3/H-Mor

The ratio of the areas under the first and second peaks is 1:2, corresponding to the expected hydrogen consumption for both processes. If LaNiO3 is the only phase present in this sample, the ratio area of the second to the first peak should be 2, however the experimental ratio is about 1.41 suggesting that a small amount of the NiO, in which Ni^{2+} are reduced to Ni^0 at about 380 °C, are also present.
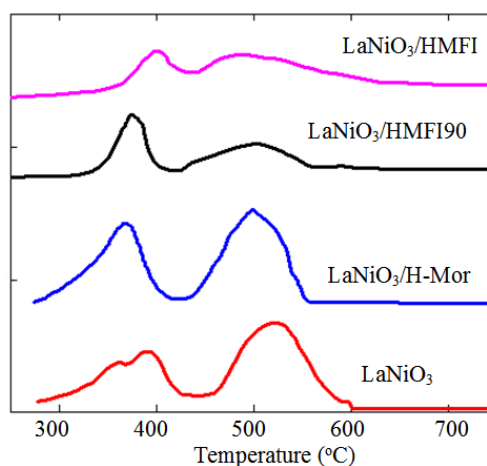
Fig. 7 TPR profiles of bulk LaNiO3 and supported LaNiO3 catalysts

In comparison with bulk LaNiO3, the ratio of area between the first and second peaks of the LaNiO3/H-MFI90, LaNiO3/H-MFI and LaNiO3/H-Mordenite was remarkably increased especially for LaNiO3/H-MFI90. That shows LaNiO3 converted to NiO (should be noted reduction temperature for this material). This is in good agreement with XRD pattern for LaNiO3/H-MFI90 sample. This behavior also has been seen in the other supports, for example SiO_2 and SBA-15 [29].

3.3 Catalyst Test

Three catalysts (LaNiO3/H-MFI90, LaNiO3/H-Mordenite and LaNiO3/H-MFI) have been tested in the fixed-bed reactor and the results of the catalytic activity tests, in terms of conversion of CH_4 and CO_2 to products and H_2/CO, are shown in Fig. 8.

As it is depicted in Fig. 8, LaNiO3/H-MFI90 catalyst showed the highest conversion of methane and CO_2. The obtained results showed that, H-MFI90 is an appropriate support for LaNiO3 perovskite catalyst.

Then, the optimum loading value for Ni has been found. For this purpose, LaNiO3/H-MFI90 (Ni Wt% = 11, 13.3 and 15.4) catalysts were prepared. The results of catalytic tests for these catalysts are shown in Fig. 9. As shown in Fig. 9, the methane conversion reaches the highest value at Ni loading 13.3 wt%.

3.4 TGA Analysis

The coke formation on the active centers during the methane dry reforming was one major reason which led to the deactivation of catalysts, resulting in low durability and activity [30]. The amount of carbon deposited on the LaNiO3, LaNiO3/H-MFI, LaNiO3/H-MFI90 and LaNiO3/H-Mordenite catalysts during the reaction was determined by TGA analysis after 75 h on stream. The thermogram is presented in Fig. 10. With increasing temperature, the samples weight

continuously decreased. The total amount of carbon deposition over the spent catalyst increased in the following sequence: $LaNiO_3/H\text{-}MFI90$ (2.14%) < $LaNiO_3/H\text{-}MFI$ (2.78%) < $LaNiO_3$ (4.31%) < $LaNiO_3/H\text{-}Mor$ (4.69%). The conditions for dry reforming of methane reaction for all samples were the same. Reaction carried out with a feed mixture composed of $CH_4/CO_2/He$ (3/3/4 vol% and total flow rate = 50 ml/min) at 750 °C. Obviously, $LaNiO_3/H\text{-}MFI90$ had a good resistance to carbon deposition in comparison with $LaNiO_3$.
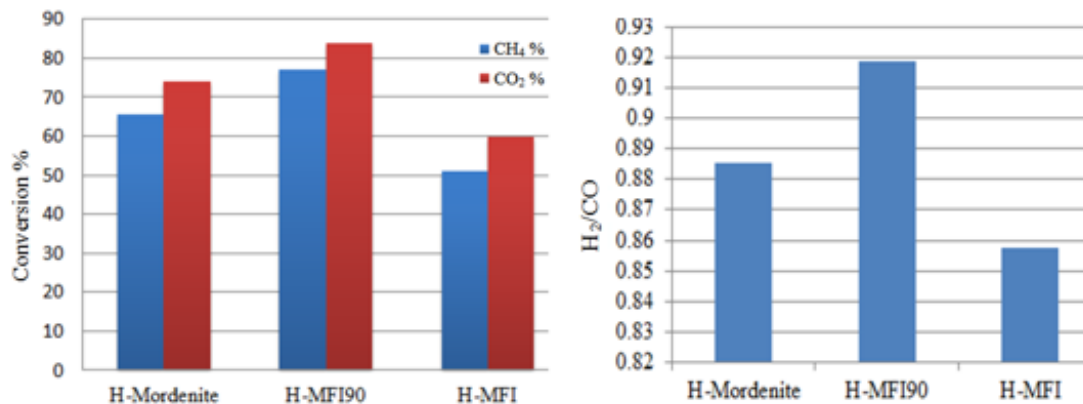
Fig. 8 Catalytic performance of $LaNiO_3/H\text{-}MFI90$, $LaNiO_3/H\text{-}Mordenite$ and $LaNiO_3/H\text{-}MFI$ catalysts, reaction condition: T = 700 °C, WHSV= 4320 mL/h·g, $CH_4/CO_2/He$ = 1:1:8
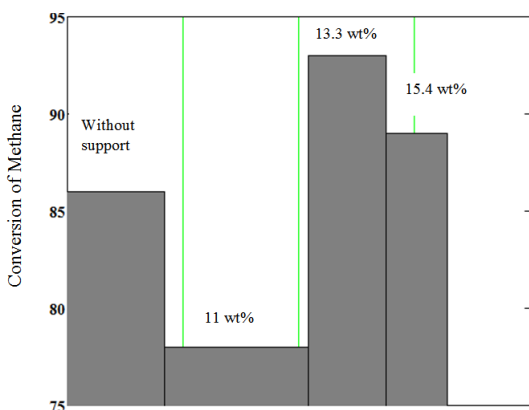
Fig. 9 Catalytic performance of $LaNiO_3/H\text{-}MFI90$ catalyst vs. Ni wt%, reaction condition: T = 700 °C, WHSV = 4320 mL/h·g, $CH_4/CO_2/He$ = 1:1:8
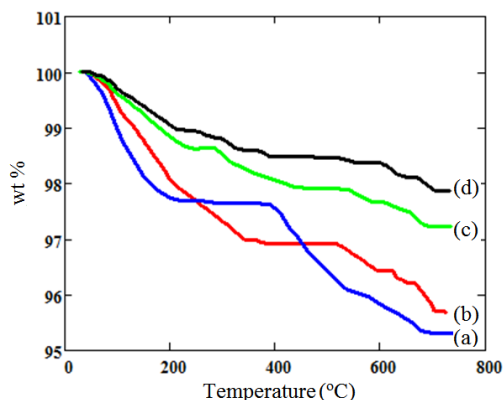
Fig. 10 TGA oxidation curve of the used (a) $LaNiO_3$, (b) $LaNiO_3/H\text{-}Mordenite$, (c) $LaNiO_3/H\text{-}MFI$ and (d) $LaNiO_3/H\text{-}MFI90$ after 75 h of reaction.

4.   Conclusion

In this paper, $LaNiO_3$ catalyst has been considered over three supports (H-MFI, H-Mordenite and H-MFI90). These supports have been compared by acidity.

The conversion of CH_4 and CO_2 to syngas was carried out by using bifunctional catalysts comprising a physical mixture of a synthesized $LaNiO_3$ catalyst and zeolites with three different inherent acidities. The results confirm that the zeolite acidity is responsible for the conversion of CH_4 and CO_2, and the formation of coke on the catalysts. These results demonstrate that the decrement of support acidity lead to better performance of catalyst in the dry reforming of methane.

It can be disclosed from the XRD test that $LaNiO_3$ perovskite formed over each of the three supports. Then, morphology of the catalyst and the distribution of concentration of element over catalyst have been investigated with applying SEM and EDX test. By comparing obtained results from EDX, it can be seen that the most amount of Ni dispersed on the catalyst support surface. This behavior also has been seen in the other supports, for example montmorillonite [31]

The XRD results showed that by using the zeolite as support, it facilitates the formation of NiO. Also, from the TPR test, it can be concluded that by using the zeolite as support, it changes the ratio of first peak's area to the second peak due to the above mentioned phase formation.

To study the $LaNiO_3$ dispersion over support surface, the TEM test was used. The obtained results of activity showed that H-MFI90 is an appropriate support for $LaNiO_3$ perovskite catalyst. When $LaNiO_3$ was loaded over zeolite, the support acidity (the Al/Si ratio) decreases and the concentration of NiO phase increases. For example, by considering XRD results and the ratio of peaks in TPR test for

LaNiO$_3$/H-MFI90 and LaNiO$_3$/H-Mordenite catalysts, it can be seen that concentration of NiO for LaNiO$_3$/H-MFI90 is more than LaNiO$_3$/H-Mordenite, indicating the important role of NiO in increasing the catalyst activity.

The methane conversion reaches the highest value at Ni loading of 13.3 wt% over this support. Perovskite structure was destroyed, and La$_2$O$_3$ and Ni^0 were formed at the conditions of reaction [32]. When LaNiO$_3$ was loaded over H-MFI90 more than 13.3 wt%, the performance of catalyst decreases. This may due to the increment of concentration La$_2$O$_3$ phase over surface of the catalyst lead to disturb interaction between Ni and H-MFI90 support [33].

The TGA results exhibited that the LaNiO$_3$/H-MFI90 sample inhibited the coke formation, and this catalyst is more stable than LaNiO$_3$.

ACKNOWLEDGEMENTS

REFERENCES

[1] J. Ross, A. van Keulen, M. Hegarty, K. Seshan, Catal. Today 30 (1996) 193.
[2] L. Bedel, A.-C. Roger, J.-L. Rehspringer, Y. Zimmermann, A. Kiennemann, J. Catal. 235 (2005) 279.
[3] M.E. Dry, Catal. Today 71 (2002) 227.
[4] H.S. Bengaard, J.K. Nørskov, J. Sehested, B. Clausen, L. Nielsen, A. Molenbroek, J. Rostrup-Nielsen, J. Catal. 209 (2002) 365.
[5] J.R. Rostrup-Nielsen, Catal. Today 71 (2002) 243.
[6] V. Tsipouriari, X. Verykios, J. Catal. 187 (1999) 85.
[7] G.S. Gallego, F. Mondragón, J.-M. Tatibouët, J. Barrault, C. Batiot-Dupeyrat, Catal. Today 133 (2008) 200.
[8] H. Wang, E. Ruckenstein, Appl. Catal. A: Gen. 204 (2000) 143.
[9] G. Valderrama, A. Kiennemann, M. Goldwasser, Catal. Today 133 (2008) 142.
[10] M.K. Nikoo, N. Amin, Fuel Process. Technol. 92 (2011) 678.
[11] G.S. Gallego, J. Barrault, C. Batiot-Dupeyrat, F. Mondragón, Catal. Today 149 (2010) 365.
[12] H. Provendier, C. Petit, J.-L. Schmitt, A. Kiennemann, C. Chaumont, J. Mater. Sci. 34 (1999) 4121.
[13] G.S. Gallego, F. Mondragón, J. Barrault, J.-M. Tatibouët, C. Batiot-Dupeyrat, Appl. Catal. A: Gen. 311 (2006) 164.
[14] C. Batiot-Dupeyrat, G. Valderrama, A. Meneses, F. Martinez, J. Barrault, J. Tatibouët, Appl. Catal. A: Gen. 248 (2003) 143.
[15] G. Moradi, M. Rahmanzadeh, S. Sharifnia, Chem. Eng. J. 162 (2010) 787.
[16] V.A. Tsipouriari, X.E. Verykios, Catal. Today 64 (2001) 83.
[17] X.E. Verykios, Int. J. Hydrogen Energy 28 (2003) 1045.
[18] G. Moradi, M. Rahmanzadeh, Catal. Commun. 26 (2012) 169.
[19] G. Valderrama, M.R. Goldwasser, C.U.D. Navarro, J.M. Tatibouët, J. Barrault, C. Batiot-Dupeyrat, F. Martínez, Catal. Today 107 (2005) 785.
[20] S. Lima, J. Assaf, M. Pena, J. Fierro, Appl. Catal. A: Gen. 311 (2006) 94-104.
[21] S. de Lima, M. Pena, J. Fierro, J. Assaf, Catal. Lett. 124 (2008) 195.
[22] G. Moradi, F. Khosravian, M. Rahmanzadeh, Chin. J. Catal. 33 (2012) 797.
[23] G. Pecchi, P. Reyes, R. Zamora, L. Cadús, J. Fierro, J. Solid State Chem. 181 (2008) 905.
[24] S.M. de Lima, J.M. Assaf, Catal. Lett. 108 (2006) 63.
[25] G.S. Gallego, C. Batiot-Dupeyrat, J. Barrault, E. Florez, F. Mondragón, Appl. Catal. A: Gen. 334 (2008) 251.
[26] I. Rivas, J. Alvarez, E. Pietri, M.J. Pérez-Zurita, M.R. Goldwasser, Catal. Today 149 (2010) 388.
[27] G. Moradi, H. Hemmati, M. Rahmanzadeh, Chem. Eng. Technol. 36 (2013) 575.
[28] J. Guo, H.Lou, Y. Zhu, X. Zheng, Mater. Lett. 57 (2003) 4450.
[29] N. Wanga, X. Yua, Y. Wanga, W. Chua, M. Liub, Catal. Today 212 (2013) 98.
[30] J.W. Hana, J.S. Parka, M.S. Choib, H. Lee, Appl. Catal. B: Environ. 203 (2017) 625.
[31] L. Li, Y. Song, B. Jiang, K. Wang, Q. Zhang, Energy 131 (2017) 58.
[32] B. Abdullah, N.A.A. Ghani, D.V.N. Vo, J. Clean. Prod. 162 (2017) 170.
[33] L. Cao, Y. Chen, W. Li, Stud. Surf. Sci. Catal. 107 (1997) 467.